



Strength, strain capacity and toughness of five dual-phase pipeline steels

Yi Ren¹ · Xian-bo Shi^{2,3} · Zhen-guo Yang^{2,3} · Yi-yin Shan^{2,3} · Wei Ye³ · Gui-xi Cai³ · Ke Yang³

Received: 24 February 2020 / Revised: 28 April 2020 / Accepted: 7 May 2020 / Published online: 16 January 2021
© China Iron and Steel Research Institute Group 2021

Abstract

The effect of microstructures on strength, strain capacity and low temperature toughness of a micro-alloyed pipeline steel was elucidated. Five various dual-phase microstructures, namely, acicular ferrite and a small amount of (around 2 vol.%) polygonal ferrite (AF + PF), polygonal ferrite and bainite (PF + B), polygonal ferrite and martensite/austenite islands (PF + M/A), polygonal ferrite and martensite (PF + M) and elongated polygonal ferrite and martensite (ePF + M), have been studied. Experimental results show that AF + PF microstructure has high yield strength and excellent low temperature toughness, whereas its yield ratio is the highest. Polygonal ferrite-based dual-phase steels, PF + B, PF + M/A and PF + M microstructures show better strain capacity and low temperature toughness. The strain capacity and low temperature toughness of ePF + M microstructure are the worst due to its high strength. The relationship between microstructure, strength, strain capacity and toughness has been established. Based on the results, the optimum microstructure for a better combination of strength, strain capacity and toughness is suggested to be the one having appropriate polygonal ferrite as second phase in an acicular ferrite matrix.

Keywords Pipeline steel · Dual-phase microstructure · Strength · Strain capacity · Toughness

1 Introduction

Pipeline steels for transportation of oil and gas have been under development for many years. The micro-alloyed pipeline steel, however, is still a research hotspot due to the increasing pipeline construction around the world [1–8]. With the rapid economic development and the continuous depletion of oil and gas resources, such hostile conditions as polar areas, ocean, geologically unstable regions and extremely low temperature environments have become common in the oil and gas exploitation, which makes it

necessary for the pipeline steels to withstand high deformability and possess low temperature crack arrest capacity, in order to make pipes have good resistance to the harsh environment during the exploitation and transportation of these products. Thus, pipeline steels are critically required to have not only high strength, high strain capacity but also good low temperature toughness simultaneously so that the pipelines run safely.

Strength, toughness and strain capacity are the most important properties for pipeline steel. In general, it is hard to keep high values of strain capacity and toughness with strength increases because they are often inversely correlated. High toughness does not mean high strain capacity, and vice versa. This is because the toughness of pipeline steel is directly related to fracture resistance [9, 10]. The strain capacity of the pipeline steel means that it cannot only meet the requirements of strength, but also have the ability of preventing the pipeline from buckling, instability and ductile fracture [11, 12]. The toughness of pipeline steel strongly depends on both the chemical composition and microstructure [13]. The nature of strain capacity of pipeline steel is mainly derived from the microstructure

✉ Xian-bo Shi
xbshi@imr.ac.cn

¹ State Key Laboratory of Metal Material for Marine Equipment and Application, Anshan 114009, Liaoning, China

² CAS Key Laboratory of Nuclear Materials and Safety Assessment, Institute of Metal Research, Chinese Academy of Sciences, Shenyang 110016, Liaoning, China

³ Institute of Metal Research, Chinese Academy of Sciences, Shenyang 110016, Liaoning, China

[11, 14]. The toughness is generally characterized by the ductile–brittle transition temperature (DBTT). The lower the DBTT is, the better the toughness is. The strain capacity of the pipeline steel is generally characterized by ratio of yield stress to tensile stress (yield ratio), uniform elongation and strain hardening exponent (n -value). Low yield ratio (< 0.8), high uniform elongation ($> 8\%$) and high n -value (> 0.1) are necessary for a high deformability pipeline steel [15].

Refinement of grain size can improve both strength and toughness of pipeline steels. It was reported that pipeline steel with single-phase acicular ferrite microstructure exhibited excellent low temperature toughness due to its finer grain size, higher dislocations density and sub-boundaries [16]. However, these are not applicable for improving the strain capacity. Grain refinement strengthening and dislocations strengthening increase the yield ratio, as a result of decreasing the strain capacity [17]. Work has shown that steels with a dual-phase microstructure, including a soft phase as matrix and a hard phase as second phase, exhibited higher strain capacity compared with single-phase microstructure [18–22]. However, the toughness of these dual-phase steels is often disappointing. The two phases might have a deleterious effect on toughness since cracks can easily nucleate at the hard phase at low temperatures [23]. There are several studies in the literature focusing on the role of microstructure on strength, strain capacity and toughness independently, but there is rarely literature focusing on the role of microstructure on them simultaneously. For this reason, it is necessary to investigate the microstructural factor on strength, strain capacity and low temperature toughness to balance three properties and optimize the microstructure design.

In the present study, five various dual-phase microstructures in a micro-alloyed pipeline steel were obtained by varying the thermo-mechanical controlled processing (TMCP) parameters. The effect of microstructure on strength, strain capacity and low temperature toughness was investigated systematically by means of tensile and impact tests, respectively. The purpose of the work is to select the candidate microstructure of pipeline steel for application in geologically unstable regions at low temperature environments.

2 Experimental

The experimental steel used in this study was produced in a laboratory scale and subjected to various rolling conditions to produce various microstructures. The chemical composition of the steel is listed in Table 1. Based on the dilatometric curves obtained by a Gleeble-3800 hot

simulator, A_{r3} and A_{r1} were determined to be 783 and 646 °C, respectively [22]. Five blocks with size of 70 mm × 70 mm × 78 mm were reheated to 1200 °C and soaked for 2 h. Seven hot rolling steps were performed within the austenite recrystallization and non-recrystallization regions to reduce the thickness from 78 to 9 mm. Five steels with different kinds of microstructures identified as A, B, C, D and E were obtained by adjusting parameters of TMCP. Steel A was cooled immediately after rolling. Steels B, C and D were air-cooled to temperature below A_{r3} . This period in the ferrite–austenite dual phase region would induce certain amount of ferrite, and subsequently the cooling rate was controlled by water spray. Steel E was finally rolled in the ferrite–austenite dual phase region, and then cooled to room temperature by water spray. The TMCP schedule is shown in Fig. 1. Table 2 shows the details of TMCP parameters, which were measured from the hot rolling experiment.

Microstructures of the experimental steels were observed by scanning electron microscopy (SEM) and optical microscopy (OM). For SEM observation, specimens taken from the transverse cross-sectional planes of the steel were firstly mechanically ground to 2000 grit by silicon carbide papers, then polished using 1 μm diamond paste suspensions, and finally etched by a 2 vol.% Nital solution. For OM observation, a two stages etching technique [24] was used to distinguish the different phases, which will be described in results section. The grain size and volume fraction of the constituent phases were analyzed by statistical image analysis.

The geometric sketch of tensile specimen with diameter of 3 mm and gauge length of 15 mm was machined from the plates perpendicular to the rolling direction. The tensile tests were conducted at room temperature with a tensile speed of 5 mm/min on a servo-hydraulic testing machine according to the GB/T228.1 standard. The yield strength ($R_{0.2}$), ultimate tensile strength (R_{UTS}), yield ratio ($R_{0.2}/R_{UTS}$) and uniform elongation of different microstructure steels were compared after the tensile test. Hollomon established the exponential equation of plastic tensile deformation based on experience in 1944 (Eq. (1)) [25]. The strain hardening exponent was got by fitting the $\ln S$ – $\ln e$ curve in plastic deformation stage according to Eq. (2).

$$S = K \cdot e^n \quad (1)$$

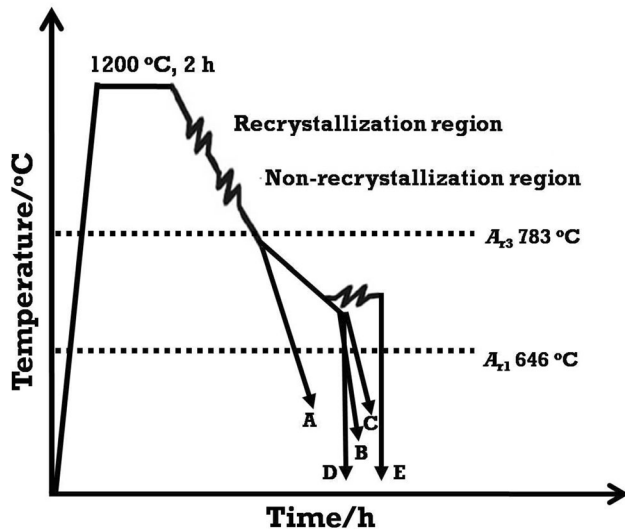
$$\ln S = \ln K + n \ln e \quad (2)$$

where S is the true stress, MPa; e is the true strain; and K is the strength coefficient, MPa. The physical and geometric meanings of n as well as the selected stress and strain data were described elsewhere [12].

Charpy impact tests were performed at temperatures of 0, – 20, – 60, – 80, – 100, – 120, – 150, – 165 and

Table 1 Chemical compositions of experimental steel (wt.%)

C	Si	Mn	S	P	Mo	Cu	Cr	Ni	Al	Nb + V + Ti	Fe
0.046	0.14	1.53	0.0014	0.0050	0.20	0.31	0.30	0.10	0.061	0.132	Balance

**Fig. 1** Schematic drawing of experimental program for TMCP

– 180 °C using the sub-size Charpy V-notch (CVN) specimens with size of 5 mm × 10 mm × 55 mm. In order to reduce errors in data interpretation, a regression analysis on CVN energy versus test temperature was done by Boltzmann fitting method [26]. Based on the data from the fitting curves, the DBTT was determined according to the average value of the upper shelf energy (USE) and the lower shelf energy (LSE).

3 Results

3.1 Microstructure characterization

Figure 2 shows the microstructures of Steels A, B, C, D and E. Steel A was cooled immediately after rolling at temperature of 772 °C, which is nearly around the A_{r3} temperature (783 °C). As a result, Steel A is characterized by acicular ferrite (AF) dominated microstructure, showing an assemblage of interwoven non-parallel ferrite (F) with non-equiaxed various-size grains distributed in random orientations. Just a small amount of polygonal ferrite (PF) distributes in AF (Fig. 2a). The relaxation process of Steels B, C, D and E was carried out, so that they present the typical dual-phase microstructures (Fig. 2b–e). In order to clearly distinguish the different phases for their microstructures, a two-stage etching technique was used [24]. The advantage of this approach is that the bainite, martensite/austenite (M/A) island and martensite phases can be easily distinguished from the ferrite matrix because they present different contrasts under optical microscopy. As shown in Fig. 3, the grey phase is bainite (Fig. 3a), and the martensite and M/A island structure looks white (Fig. 3b–d). Thus, it can be confirmed that Steel B consists of polygonal ferrite and bainite (B). Steel C is mainly composed of PF and a small amount of M/A islands surrounded by the ferrite matrix. Both Steels D and E exhibit a dual-phase microstructure including polygonal ferrite and martensite (M) because of high cooling rate after relaxation. The difference of them is that elongated polygonal ferrite (ePF) and martensite are present in Steel E due to rolling in the ferrite–austenite dual phase region finally, whereas Steel D reveals blocky PF + M microstructure.

Table 2 Processing parameters in TMCP for experimental steel

Steel	Interpass reduction distribution (mm) and rolling temperature (°C)							Accelerated cooling	
	78 → 62	62 → 45	45 → 30	30 → 24	24 → 16	16 → 11	11 → 9	Start and end temperatures/°C	Cooling rate/(°C s ⁻¹)
A	1100			892			772	772 → 430	16
B	1086			915			761	691 → 411	27
C	1069			903			768	686 → 399	20
D	1056			909			786	675 → RT	> 50
E	1052			880			715	715 → RT	> 50

RT Room temperature

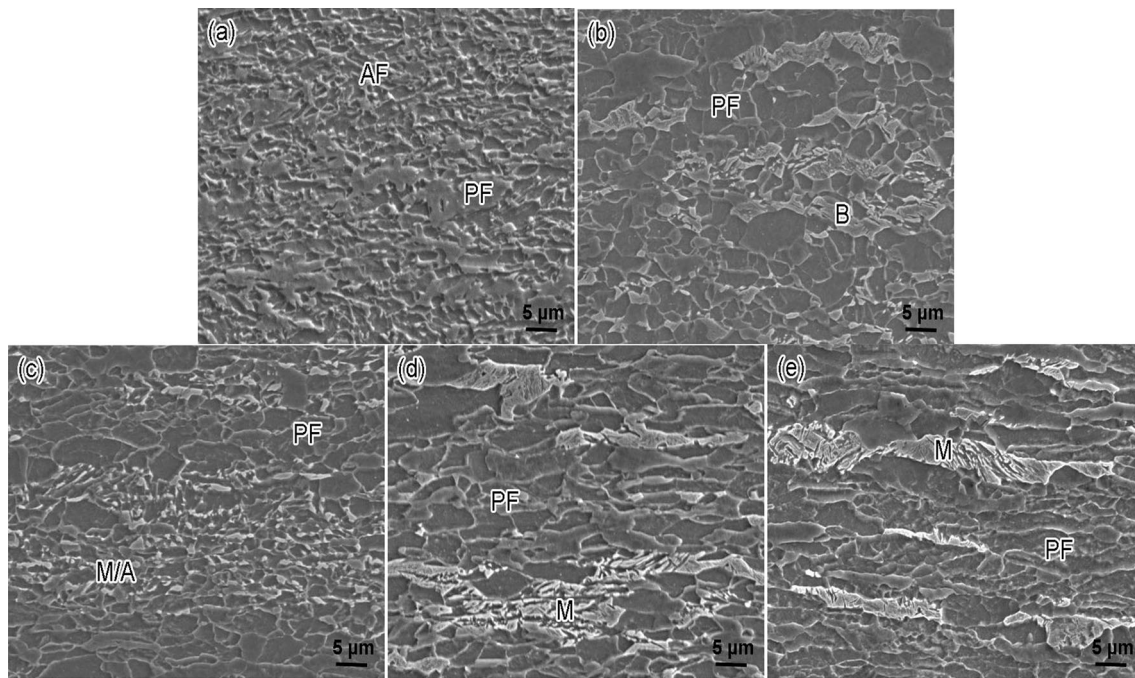


Fig. 2 SEM microstructures of experimental steels. **a** Steel A; **b** Steel B; **c** Steel C; **d** Steel D; **e** Steel E

Detailed microstructure characteristics of five steels are summarized in Table 3. Ferrite grain size of Steel A ranges from 2 to 5 μm , the average grain size is 2.3 μm , and the Steel A also contains a small amount of PF (around 2 vol.%). The ferrite grain size of Steel B varies in the range of 2–13 μm , and the volume fraction of bainite is 20.2%. The Steel C, with a relatively lower cooling rate, is mainly composed of 95.5% ferrite and 4.5% M/A islands. It has similar range of ferrite grain size to Steels B and D. Steels D and E show the same microstructure of F + M, and the volume fractions of martensite in Steels D and E are 10.6% and 9.1%, respectively. Steel E has a wider range of ferrite grain size due to rolling in the dual phase region, which makes ferrite grain elongate. The average ferrite grain size is 5.1, 4.3, 6.4 and 7.7 μm for Steels B, C, D and E, respectively, which are bigger than that of Steel A.

3.2 Tensile properties

Figure 4 shows the true stress–strain curves of five steels. They all show round-roof shape and exhibit continuous yielding behavior, which is an important feature for high deformability pipeline steel [11, 27]. The $R_{10.2}$, R_{UTS} , $R_{10.2}/R_{UTS}$, uniform elongation and total elongation are shown in Table 4. It can be found that the yield ratio and uniform elongation of Steels B, C and D can meet the requirements of high deformability pipeline steel [15]. The yield ratios of Steels A and E are 0.86 and 0.83, respectively, which are above 0.8 and they cannot meet the target that below 0.8

[15]. The Steels B and C have similar yield strength, whereas the R_{UTS} of Steel C is relatively higher than that of Steel B. Obviously, finer average grain size in Steel C is not the direct reason, because grain refinement strengthening is dominated by increasing yield strength [17]. The result can be interpreted from the fact that the second phase M/A island is a very hard phase [11], leading to a higher R_{UTS} . Compared with Steels B and C, Steel A with AF dominated microstructure has finer grain size (Fig. 2a and Table 3). Besides, acicular ferrite has higher dislocation density compared with PF [28]. Grain refinement strengthening and dislocation strengthening can increase the $R_{10.2}$ and R_{UTS} [17]. Thus, Steel A has higher $R_{10.2}$ and R_{UTS} . Steel D shows lower $R_{10.2}$ but higher R_{UTS} . It can be easily understood that the $R_{10.2}$ is decreased because of coarsening of ferrite grain size, and the R_{UTS} is increased due to the martensite produced by fast cooling rate (Table 2). Martensite contains a large amount of dislocations in the microstructure, which causes a significant strengthening effect. Steel E has bigger ferrite grain size and less martensite compared with Steel D (Table 3). In ferrite–martensite dual-phase steels, soft ferrite ensures high formability, whereas hard martensite enhanced strength [29]. Moreover, the R_{UTS} is mainly dependent on the volume fraction of hard phase [14]. It means that Steel E should have shown lower strength than Steel D. However, the result is contrary (Table 4). The $R_{10.2}$ and R_{UTS} of Steel E are remarkably improved after rolling in the dual-phase region, indicating that a large amount of dislocations must be produced in Steel E. The dislocation strengthening

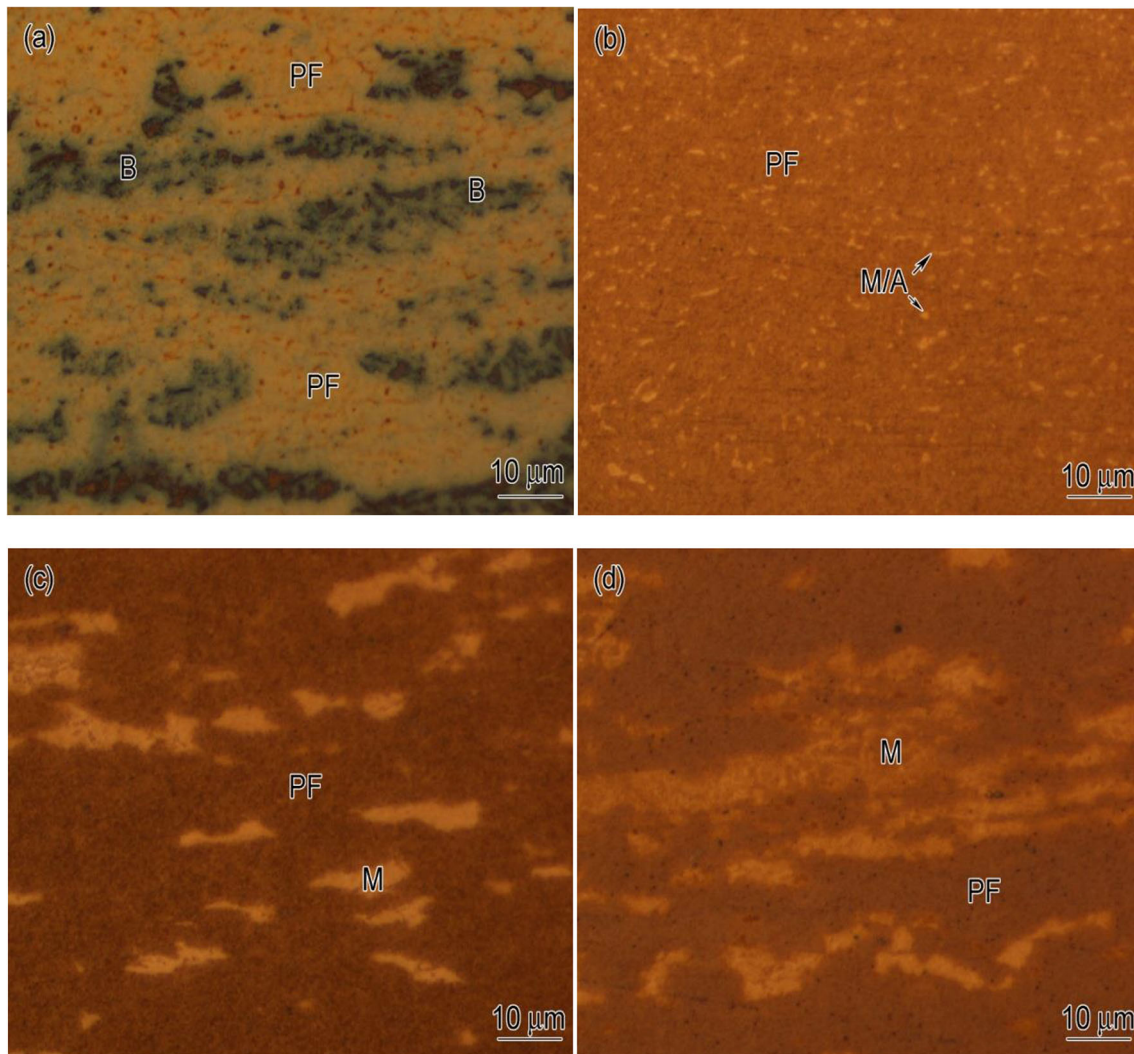


Fig. 3 Optical microstructures of experimental steels. **a** Steel B; **b** Steel C; **c** Steel D; **d** Steel E

Table 3 Details of microstructure features of experimental steels

Steel	Microstructure type	Ferrite grain size/ μm	Average grain size/ μm	Volume fraction of second phase/%
A	AF + PF	2–5	2.3	AF 98.8, PF 1.8
B	PF + B	2–13	5.1	PF 79.8, B 20.2
C	PF + M/A	2–14	4.3	PF 95.5, M/A 4.5
D	PF + M	2–15	6.4	PF 89.4, M 10.6
E	ePF + M	2–21	7.7	ePF 90.9, M 9.1

can increase the $R_{0.2}$ and R_{UTS} simultaneously [17] and therefore makes the $R_{0.2}$ and R_{UTS} higher.

Figure 5 shows the $\ln S$ – $\ln \epsilon$ curves of five steels. The slope of $\ln S$ – $\ln \epsilon$ curves is n -value. It can be found the slopes are nonlinear. It means that the n -value changes at different plastic strain stages. To further analyze the

variation of n -value at different strain stages, the curves of instantaneous n -value versus engineering strain are plotted in Fig. 6. The variation of n -value of five steels shows a common feature, that is, there is an obvious peak value at a certain engineering strain. At the beginning of plastic deformation, the n -value increases with the increase in

plastic strain. It reaches the highest values of 0.115, 0.176, 0.153, 0.157 and 0.103 at the engineering strain of 4.5%, 4.1%, 3.3%, 3.3% and 3.8% for Steels A, B, C, D and E, respectively. The n -value decreases with further increase in the plastic strain, indicating that strain hardening ability decreases.

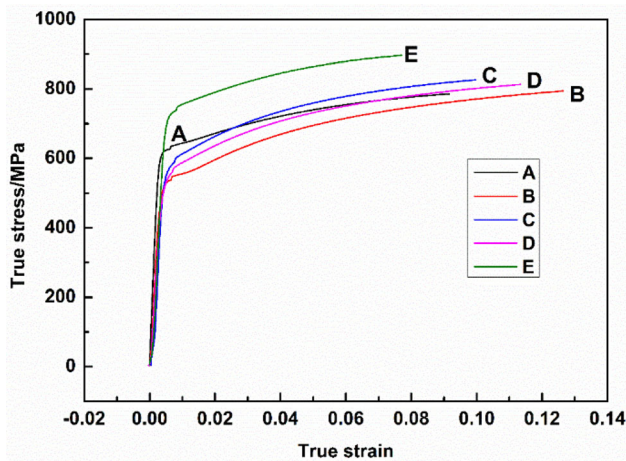


Fig. 4 True stress–strain curves of experimental steels

Table 4 Tensile properties of experimental steels

Microstructure	$R_{10.2}$ /MPa	R_{UTS} /MPa	$R_{10.2}/R_{UTS}$	Elongation/%	Uniform elongation/%
A	620	717	0.86	23.5	9.5
B	515	700	0.74	28.0	13.6
C	516	747	0.69	25.0	11.4
D	502	725	0.69	26.0	12.8
E	689	830	0.83	20.0	7.9

Although the n -value is variable in dual-phase and multi-phase steels, the average n -value generally is obtained to compare the strain capacity by fitting the $\ln S$ – $\ln e$ curve according to Hollomon equation (Eq. (2)) [27]. Figure 7 shows the fitting curves, which are divided into two sections. Obviously, there are two slopes for both cases, indicating two average n -values (n_1 and n_2). Table 5 lists the average n -values for five steels. At the beginning of plastic deformation, the average n -values (n_2) of five steels are relatively low, which means relatively weak strain hardening capacity. At this stage, the higher the n_2 is, the faster the strength increases. However, n_1 becomes higher for further deformation. It means that strain hardening ability becomes strong. At low strain level, it is sure that microstructures with PF + M/A islands and PF + M show the higher strain hardening exponent (n_2 -value), and the n_2 -value of Steel B with PF + B microstructure is good; however, the n_2 -value of Steel A with AF plus a small amount of PF is the lowest. Compared with Steel D with blocky PF + M microstructure, Steel E with ePF + M shows lower n_2 -value. At high strain level, Steel B exhibits the highest strain hardening exponent (0.158). Steels D (0.143), C (0.139), A (0.105) and E (0.096)

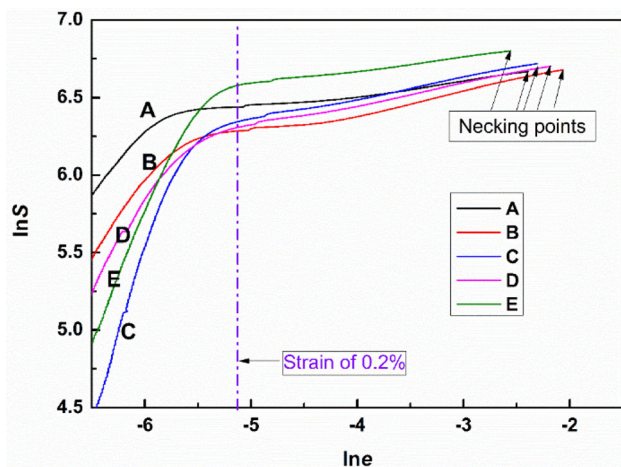


Fig. 5 $\ln S$ – $\ln e$ curves of experimental steels

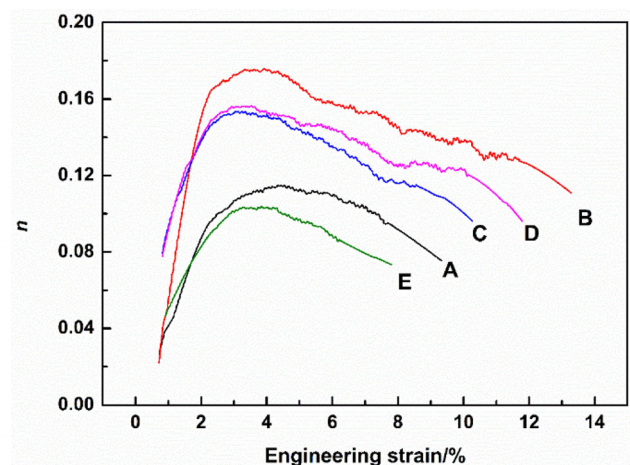


Fig. 6 Curves of instantaneous n -value versus engineering strain of experimental steels

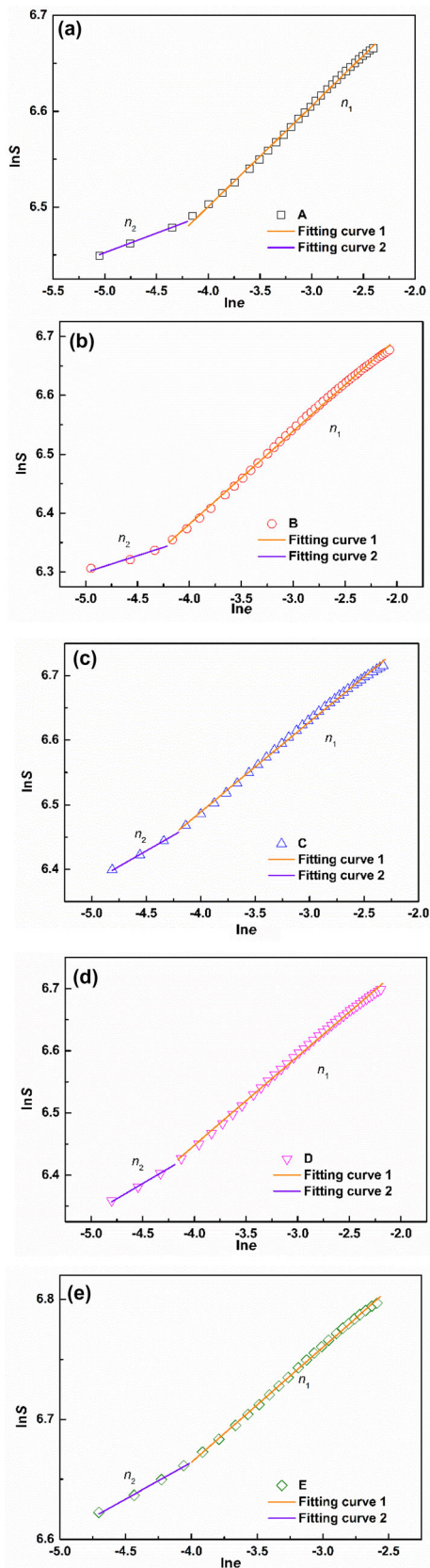


Fig. 7 Hollomon analysis of experimental steels. **a** Steel A; **b** Steel B; **c** Steel C; **d** Steel D; **e** Steel E

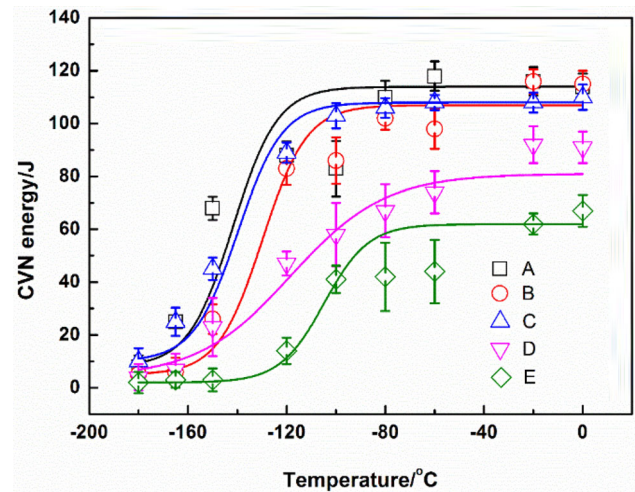


Fig. 8 Charpy V-notch impact energy versus test temperatures along with Boltzmann function fitting based on experimental data

Table 5 Strain hardening exponents of experimental steels

Strain hardening exponent	A	B	C	D	E
n_1	0.105	0.158	0.139	0.143	0.096
n_2	0.041	0.057	0.097	0.098	0.061

decrease one by one. The n -value is used to characterize the strain capability of plastic deformation in high deformability pipeline steel. The higher the value of n , the better the strain capacity, and the stronger the resistance to plastic deformation. Therefore, Steels B, C, and D show better resistance to plastic deformation, and it is more notable at high strain level.

3.3 Low temperature impact toughness

To compare the low temperature toughness of experimental steels with various dual-phase microstructures, the curves of CVN energy versus temperatures for five steels are plotted in Fig. 8. Table 6 shows the data of USE, LSE and DBTT obtained from Fig. 8. Steel A shows the best low temperature toughness, with the highest USE above 110 J and the lowest DBTT below -140 °C. The fact is attributed to its microstructure. Excellent low temperature toughness of the AF pipeline steel has been proved resulting from its finer effective grain size, higher content of low angle grain boundaries and its more bent crack propagation path in the fracture [16]. Compared with AF microstructure, steels with dual-phase microstructure show relatively low impact toughness. The USE of five steels is decreased in the order of A, C, B, D and E. Steel C with PF + M/A islands exhibits optimum low temperature toughness for all steels with dual-phase microstructure,

Table 6 Charpy V-notch impact energy of experimental steels

Microstructure	Upper shelf energy/J	Lower shelf energy/J	DBTT/°C
A	114	4	- 142
B	107	5	- 129
C	108	10	- 139
D	81	4	- 118
E	62	2	- 104

and Steel B with PF + B microstructure is second. The impact toughness of steels with PF + M is not good, and Steel D is superior to Steel E. According to the results of regression analysis, the DBTT values were estimated as - 142, - 139, - 129, - 118, and - 104 °C for Steels A, C, B, D and E, respectively.

4 Discussion

It is believed that the strain capacity of the steel is improved by lowering the yield ratio, increasing the n -value and uniform elongation. As shown in Fig. 9, the steels show that different combinations of strain capacity and low temperature toughness depend on their various microstructures. The effect of microstructure on strain capacity and impact toughness is remarkable. In general, it can be said that steel with better toughness should has higher value of elongation. However, such statement may lead to a wrong conclusion since toughness is a function of not only elongation but also strength. In the case of Steel A, the low temperature toughness is the best and it shows higher yield strength. But the uniform elongation is relatively lower than that of Steels B, C and D, which means that it is difficult to keep adequate values of toughness and elongation as strength increases to a higher level (Fig. 9a). Steel A is mainly composed of AF and just a small amount of PF (around 2 vol.%), which is not a typical dual-phase

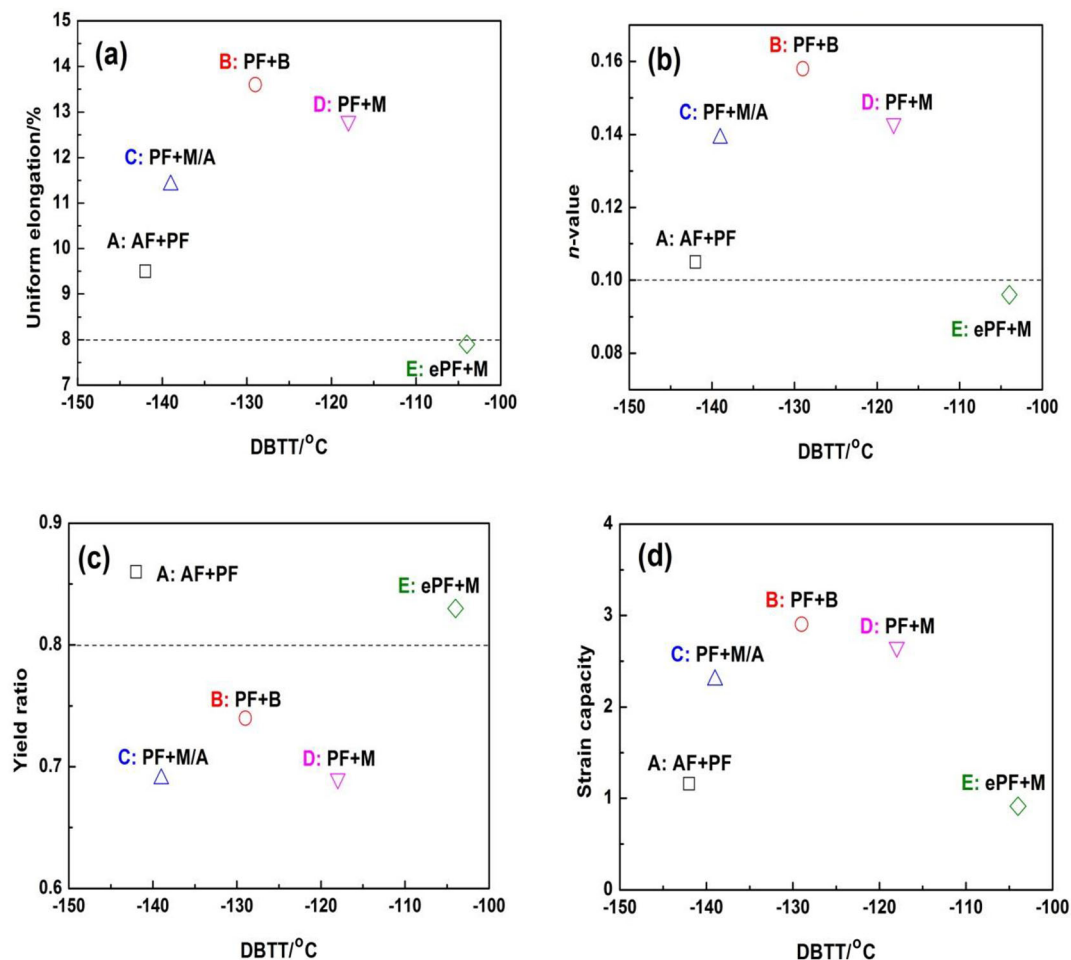


Fig. 9 Relationship between strain capacity and DBTT of various microstructure steels. **a** Uniform elongation versus DBTT; **b** n -value (n_1) versus DBTT; **c** yield ratio versus DBTT; **d** strain capacity versus DBTT

microstructure (Fig. 2a). AF has been proved to be the optimum microstructure in high performance pipeline steel due to its good combination of strength and toughness [30]. This is attributed to its finer grain size and higher dislocation density. However, finer grain size increases the yield strength dramatically, as a result of accompanying increase in yield ratio [12]. In addition, finer grain size decreases the work hardening rate, which has an additional effect on increasing yield ratio [23]. Thus, AF microstructure has the highest yield ratio (Fig. 9c), which leads to a low uniform elongation (Fig. 9a). Accordingly, the n -value is relatively low (Fig. 9b). One of the ways of enhancing the strain capacity is the utilization of hard second phase in the microstructure, and the larger difference in the strength between the soft matrix phase and the hard second phase is more desirable to obtain good strain capacity [23]. This strategy is confirmed in cases of Steels B, C and D, and they have relatively higher uniform elongation (Fig. 9a), higher n -value (Fig. 9b) and lower yield ratio (Fig. 9c) compared with Steel A.

In order to clearly compare the strain capacity of steels with dual-phase microstructure, the strain capacity is defined in the present study as follows:

$$\text{Strain capacity} = \frac{\text{UE} \times N}{\text{YR}} \quad (3)$$

where UE is uniform elongation, %; N is the n -value; and YR is yield ratio. Taking the corresponding experimental values of five steels, a scatter plot of strain capacity versus DBTT can be made, as shown in Fig. 9d. It can be observed that the strain capacity of Steel B with PF + B microstructure is the best, PF + M is second, PF + M/A islands is third and Steel E with ePF + M microstructure is the worst. For low temperature toughness, however, Steels C, B, D and E decrease one by one. Steel C with PF + M/A microstructure shows the best low temperature toughness in dual-phase microstructure. In addition, it can be found that the strain capacity of steels with the same microstructure may also be different. Zhao et al. [3] believed that the ferrite–bainite dual-phase steel with banded bainite possessed better deformation compatibility than that with equiaxed bainite. In ferrite–martensite dual-phase steel, the fibrous martensite was reported to behave the best combination of strength and ductility than banded and island-shaped martensite. The shape, size and distribution of second phase could play an important role in deformation compatibility [29]. In the present study, Steel D with blocky martensite shows better strain capacity and toughness compared with Steel E with banded martensite. There is no doubt that martensite morphology is one of the factors influencing the strain capacity. However, the higher strength of Steel E is also an important factor since the strength and strain capacity is often inversely correlated.

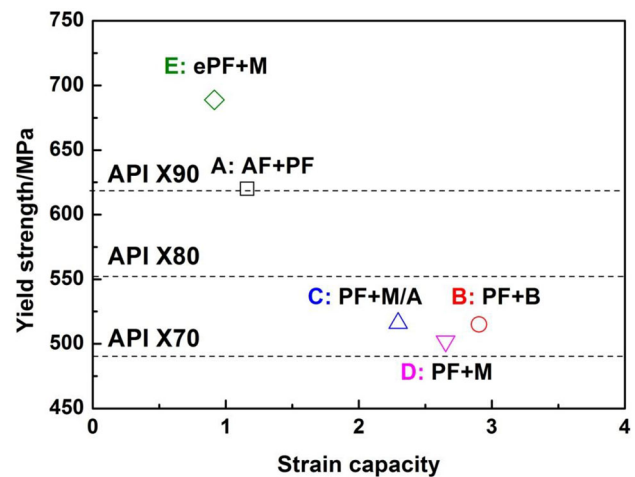


Fig. 10 Relationship between strain capacity and yield strength of various microstructure steels

As shown above, based on the correlation of microstructure, strain capacity and toughness, it can be concluded that the optimum microstructure for high deformability pipeline steel application at low temperature environment should be the one having hard second phase in PF matrix (Steels B, C and D). Unfortunately, their yield strength is not enough (Fig. 10). In other words, in addition to strain capacity and toughness for pipeline steel, the high yield strength is also necessary. However, the relationship between strength and strain capacity is often opposite, that is, an increase in the strain capacity is achieved at the expense of the strength. The achievement of optimum combination of strength and strain capacity is difficult in PF-based dual-phase steels. AF-based steel has the advantage of high yield strength and excellent low temperature toughness. According to the empirical law of dual-phase steel, it is rational to believe that the best combination of strength, strain capacity and DBTT can be overcome by introduction of PF with appropriate volume fraction as second phase in AF matrix. Future studies regarding the optimal ratio between PF and AF on strength, strain capacity and toughness would be interesting to have a complete understanding of this microstructure.

5 Conclusions

1. AF with a small amount of PF microstructure exhibits high yield strength and excellent low temperature toughness, whereas its yield ratio is the highest, which cannot meet the requirement of strain capacity.
2. For dual-phase steels, PF + B, PF + M/A, and PF + M microstructures, show better strain capacity and good low temperature toughness.

3. The strain capacity and low temperature toughness of ePF + M microstructure are the worst, which is mainly due to the highest strength produced by rolling in the ferrite–austenite dual phase region.
4. The optimum microstructure for a better combination of strength, strain capacity and toughness is suggested to be the one having more volume fraction of polygonal ferrite as second phase in an acicular ferrite matrix.

Acknowledgements This work was financially supported by the National Key Research and Development Program of China (Grant Nos. 2017YFB0304901, 2018YFC0310302 and 2018YFC0310304), State Key Laboratory of Metal Material for Marine Equipment and Application Funding (Grant No. SKLMEA-K201901) and the Doctoral Scientific Research Foundation of Liaoning Province (Grant No. 20180540083).

References

- [1] S.J. Jia, B. Li, Q.Y. Liu, Y. Ren, S. Zhang, H. Gao, J. Iron Steel Res. Int. (2020) <https://doi.org/10.1007/s42243-019-00346-3>.
- [2] A. Gervasyev, I. Pyshmintsev, R. Petrov, C. Huo, F. Barbaro, Mater. Sci. Eng. A 772 (2020) 138746.
- [3] Z.T. Zhao, X.S. Wang, G.Y. Qiao, S.Y. Zhang, B. Liao, F.R. Xiao, Mater. Des. 180 (2019) 107870.
- [4] B. Li, Q.Y. Liu, S.J. Jia, Y. Ren, B. Wang, Acta Metall. Sin. (Engl. Lett.) 31 (2018) 1038–1048.
- [5] X.B. Shi, W. Yan, D. Xu, M.C. Yan, C.G. Yang, Y.Y. Shan, K. Yang, J. Mater. Sci. Technol. 34 (2018) 2480–2491.
- [6] X.D. Li, C.N. Li, G. Yuan, G.D. Wang, Acta Metall. Sin. (Engl. Lett.) 30 (2017) 483–491.
- [7] X.B. Shi, W. Yan, M.C. Yan, W. Wang, Z.G. Yang, Y.Y. Shan, K. Yang, Acta. Metall. Sin. (Engl. Lett.) 30 (2017) 601–613.
- [8] X.B. Shi, W. Yan, W. Wang, Y.Y. Shan, K. Yang, Mater. Des. 92 (2016) 300–305.
- [9] L.W. Tong, L.C. Niu, S. Jing, L.W. Ai, X.L. Zhao, Thin Wall Struct. 132 (2018) 410–420.
- [10] Y. Zhao, X. Tong, X.H. Wei, S.S. Xu, S. Lan, X.L. Wang, Z.W. Zhang, Int. J. Plasticity 116 (2019) 203–215.
- [11] T. Shinmiya, N. Ishikawa, M. Okatsu, S. Endo, N. Shikanai, Int. J. Offshore Polar Eng. 18 (2008) 308–313.
- [12] X.B. Shi, W. Yan, Z.G. Yang, Y. Ren, Y.Y. Shan, K. Yang, ISIJ Int. 60 (2020) 792–798.
- [13] B.X. Wang, J.B. Lian, Mater. Sci. Eng. A 592 (2014) 50–56.
- [14] C.J. Tang, C.J. Shang, S.L. Liu, H.L. Guan, R.D.K. Misra, Y.B. Chen, Mater. Sci. Eng. A 731 (2018) 173–183.
- [15] X.Y. Zhang, H.L. Gao, X.Q. Zhang, Y. Yang, Mater. Sci. Eng. A 531 (2012) 84–90.
- [16] W. Wang, Y.Y. Shan, K. Yang, Mater. Sci. Eng. A 502 (2009) 38–44.
- [17] Q.L. Yong, Secondary phases in steels, Metallurgical Industry Press, Beijing, China, 2006.
- [18] T. Hüper, S. Endo, N. Ishikawa, K. Osawa, ISIJ Int. 39 (1999) 288–294.
- [19] N. Ishikawa, N. Shikanai, J. Kondo, JFE Tech. Rep. 12 (2008) 15–19.
- [20] M. Okatsu, N. Shikanai, J. Kondo, JFE Tech. Rep. 12 (2008) 8–14.
- [21] R.T. Li, X.R. Zuo, Y.Y. Hu, Z.W. Wang, D.X. Hu, Mater. Charact. 62 (2011) 801–806.
- [22] X.B. Shi, W. Yan, W. Wang, L.Y. Zhao, Y.Y. Shan, K. Yang, J. Iron Steel Res. Int. 22 (2015) 937–942.
- [23] Y.M. Kim, S.K. Kim, Y.J. Lim, N.J. Kim, ISIJ Int. 42 (2002) 1571–1577.
- [24] R.M. Alé, J.M.A. Rebello, J. Charlier, Mater. Charact. 37 (1996) 89–93.
- [25] J.H. Hollomon, Trans. ASM 32 (1944) 123–133.
- [26] Y. Sakai, K. Tamanoi, N. Ogura, Nucl. Eng. Des. 115 (1989) 31–39.
- [27] L.K. Ji, H.L. Li, H.T. Wang, J.M. Zhang, W.Z. Zhao, H.Y. Chen, Y. Li, Q. Chi, J. Mater. Eng. Perform. 23 (2014) 3867–3874.
- [28] M.C. Zhao, K. Yang, Y.Y. Shan, Mater. Lett. 57 (2003) 1496–1500.
- [29] D. Das, P.P. Chattopadhyay, J. Mater. Sci. 44 (2009) 2957–2965.
- [30] F. Xiao, B. Liao, D.L. Ren, Y.Y. Shan, K. Yang, Mater. Charact. 54 (2005) 305–314.